Crystallisation of magmatic topaz and implications for Nb-Ta-W mineralisation in F-rich silicic melts – The Ary-Bulak ongonite massif

Andrea Agangi[1,2], Vadim S. Kamenetsky[2], Axel Hofmann[1], Wojciech Przybyłowicz[3,4], Nikolay V. Vladykin[5]

[1]PaleoProterozoic Mineralisation Group, University of Johannesburg, Auckland Park 2006, South Africa, tel. +27(0)11 559 4087

[2]ARC Centre of Excellence in Ore Deposits and School of Earth Sciences, University of Tasmania, Hobart, TAS 7001, Australia

[3] Materials Research Department, iThemba LABS, National Research Foundation, Somerset West 7129, South Africa

[4] AGH University of Science and Technology, Faculty of Physics & Applied Computer Science, Al. A. Mickiewicza 30, 30-059 Krakow, Poland

[5] Vinogradov Institute of Geochemistry and Analytical Chemistry, SB RAS, Irkutsk, Russia

Abstract

Textural, mineralogical and geochemical data on F-rich rhyolite (ongonite) from the Ary-Bulak massif of eastern Transbaikalia help constraining the formation of magmatic topaz. In these rocks, topaz occurs as phenocrysts, thus providing compelling evidence for crystallisation at the orthomagmatic stage. Cathodoluminescence images of topaz and quartz reveal growth textures with multiple truncation events in single grains, indicative of a dynamic system that shifted from saturated to undersaturated conditions with respect to topaz and quartz. Electron microprobe and Raman analyses of topaz indicate near-pure F composition [$Al_2SiO_4F_2$], with very limited OH replacement. Laser ablation ICP-MS traverses revealed the presence of a large number of trace elements present at sub-ppm to hundreds ppm levels. The chemical zoning of topaz records trace element fluctuations in the coexisting melt. Concentrations of some trace elements (Li, Ga, Nb, Ta and W) are correlated with cathodoluminescence intensity, thus suggesting that some of these elements act as CL activators in topaz. The study of melt inclusions indicates that melts with different F contents were trapped at different stages during formation of quartz and topaz phenocrysts, respectively. Electron microprobe analyses of glass in subhedral quartz-hosted melt inclusions indicate F ≤1.2 wt.%, whereas irregular-shaped melt inclusions hosted in both topaz and quartz have F ≤9 wt.%. Cryolithionite [$Na_3Li_3Al_2F_{12}$] coexists with glass in irregular inclusions, implying high Li contents in the melt. The very high F contents would have increased the solubility of Nb, Ta and W in the melt, thus allowing progressive concentration of these elements during magma evolution. Crystallisation of Nb-Ta-W-oxides (W-ixiolite and tantalite-columbite) may have been triggered by separation of cryolithionite, which would have caused F and Li depletion and consequent drop in the solubility of these elements.

1. Introduction

Topaz [$Al_2SiO_4(F,OH)_2$] commonly occurs in cavities in F-rich felsic igneous rocks, quartz veins and greisens associated with felsic intrusions (Burt et al., 1982; Kortemeier and Burt, 1988). In many instances, topaz is interpreted as crystallising in the last stages (pneumatolitic stage) of evolution of magmatic-hydrothermal systems (e.g. from gas-filled cavities in volcanic rocks, Christiansen et al., 1983), or as a product of metasomatism and autometamorphism (Haapala, 1977; Lukkari, 2002). In metamorphic rocks, OH-rich varieties of topaz are stable at ultra-high pressure and high temperature (12 GPa, 1100˚C; Alberico et al., 2003; Zhang et al., 2002). However, evidence for topaz formation in the orthomagmatic stage has been presented in some strongly fractionated, F-rich felsic igneous rocks (Haapala and Lukkari, 2005; Naumov et al., 1991; Thomas et al., 2005; 2009; Webster et al., 2004). In some intrusive rocks, such as pegmatite, the magmatic origin of topaz is indicated by the presence of topaz-hosted melt inclusions (e.g. the Kymi granite; Haapala, 1977; Lukkari et al., 2009; or dykes in the Eurajoki Rapakivi Granite Stock; Haapala and Thomas, 2000) and by the simultaneous trapping of topaz and melt in quartz (Thomas et al., 2009). In volcanic rocks, topaz mostly occurs in the groundmass (Burt et al., 1982; Gioncada et al., 2014; Štemprok, 1991), sometimes making the interpretation of its origin difficult, and only rarely as phenocrysts (Kovalenko et al., 1971). Experiments have demonstrated that topaz can crystallise from low-Ca, peraluminous silicate melts containing as little as 1 wt.% F (Christiansen and Lee, 1986), or higher (F ≥1.7 wt.%; Dolejš and Baker, 2007, or F ≥2 – 3 wt.%; Lukkari and Holtz, 2007).

Ongonites are a special type of extremely F-rich rhyolites (F up to 1.5 – 2 wt.% in whole-rock analyses) with Na/K >1, which contain phenocrysts of feldspar, quartz, minor mica and, in some cases, topaz (Kovalenko and Kovalenko, 1976; Peretyazhko et al., 2011). These rocks are considered to be the volcanic equivalent of topaz-bearing granites (Letnikov, 2008). Ongonites have first been described in Mongolia and Russia (Kovalenko et al., 1971), and similar rocks of Cenozoic age have been described in the American Cordillera of the USA and Mexico (Burt et al., 1982; Christiansen et al., 1984; Congdon and Nash, 1988; Kortemeier and Burt, 1988), and they are in some cases associated with topazite (quartz-topaz rock) dykes. These rocks typically occur in extensional, intraplate/post-collisional settings (Burt et al., 1982;

Kovalenko et al., 2007; Taylor, 1992). Ongonites and other strongly fractionated, topaz-bearing rocks are known to be enriched in Li, B, Sn, Zn, W, Mo and U, other than Nb-Ta, to concentrations that can amount to ore deposits (Antipin et al., 2006; Burt et al., 1982; Christiansen and Lee, 1986; Haapala, 1997; Syritso et al., 2012; Taylor, 1992; Moghazi et al., 2011). Niobium-Ta oxides, such as the columbite-tantalite solid solution series and ixiolite, deposited as magmatic accessory phases and in alteration zones around F-rich intrusions, account for most of the current production of these elements worldwide (Melcher et al., 2014).

This study is focussed on a single ongonite sample from the Ary-Bulak massif, Transbaikalia, Russia (Naumov et al., 1971) containing topaz as euhedral phenocrysts, up to 1 – 2 mm in size, and as elongate microlites (up to 100 μm in length) in the groundmass. The close association of Nb-Ta-(W) oxide with topaz observed in the Ary-Bulak massif (Kovalenko et al., 1975; Peretyazhko et al., 2011) suggests a link between concentrations of these elements and the formation of topaz. Both topaz and quartz phenocrysts host melt inclusions, which can record the evolution of the melt through different stages of crystallisation, and provide evidence of the nature and composition of melt(s) present at the moment of topaz crystallisation. We use detailed textural and microchemical data to gain insight into the formation of topaz in felsic magmatic systems. We show that the CL and chemical zoning of topaz reflect complex processes, and can be used as a proxy for the trace element composition of the parent melt. Our findings have implications on the origin of Nb-Ta-(W) ore deposits associated with F-rich magmas.

2. Geological setting

The 142 ±0.7 Ma old (Kostitsyn et al., 1996) Ary-Bulak massif forms a laccolith, 700 × 1500 m in size, intruding Late Jurassic-Early Creataceous shales and limestones of the Ust’-Boryza Formation and basalt (Antipin et al., 2009; Kovalenko and Kovalenko, 1976; Peretyazhko and Savina, 2010b). The centre of the Ary-Bulak massif consists of porphyritic ongonite with up to 20 vol.% phenocrysts of sanidine, albite, quartz, Li-mica (zinnwaldite) and occasional topaz. The fine-grained groundmass mostly contains quartz, feldspar and topaz. These rocks contain up to 1.5 wt.% F (Kovalenko et al., 1975; Peretyazhko et al., 2011). To the southwest, the porphyritic rocks grade into an aphanitic variety of ongonite, which forms a quenched contact zone up to 100 m wide (Peretyazhko et al., 2011). These rocks contain rare phenocrysts of quartz and sanidine, and prosopite [$CaAl_2F_4(OH)_4$] (Peretyazhko et al., 2011). Whole-rock analyses indicate strong enrichment in Nb, Ta, W, Sn, Li and Rb in comparison with average continental crust (e.g. up to 73 ppm Nb, 48 ppm Ta, 30 ppm W, respectively), and typically flat or concave upwards primitive-mantle normalised rare earth element (REE) patterns with pronounced negative Eu anomalies (e.g. Syritso et al., 2012). Even higher concentrations of these elements have been measured in melt inclusions (Nb up to 180 ppm, Li up to 698 ppm; Peretyazhko and Savina, 2010b). The massif was emplaced at the same time as other shallow intrusions of similar composition in Eastern Transbaikalia (Khrangilay complex, Badanina et al., 2006). Evidence for the presence of different immiscible saline fluids, brines and melts, including silicate, Ca-fluoride, Mg-fluoride (MgF_2) and aluminofluoride melts in the Ary-Bulak massif, has been provided by inclusion studies (Peretyazhko and Savina, 2010a; 2010b; Peretyazhko et al., 2007b). Further, anomalous Cs and As concentrations (up to 17 wt.% Cs) were reported in some quartz-hosted silicate melt inclusions (Peretyazhko et al., 2007a; Peretyazhko and Savina, 2010a). A glass derived by quenching of the CaF melt is also abundant in the groundmass of aphanitic and some porphyritic samples, and results in a positive Ca – F correlation and locally extremely high F contents (up to ~19 wt.%; Peretyazhko et al., 2011). Small (up to 5 µm) quartz-hosted silicate melt inclusions homogenise at 650 – 750˚C (Peretyazhko et al., 2011), although larger inclusions either homogenise at much higher temperatures (around 1000˚C) or do not homogenise, possibly due to decrepitation.

3. Sample preparation and analytical techniques

A sample of topaz-phyric ongonite from the central part of the Ary-Bulak massif (sample AB1) has been studied in thin section by optical microscopy, back-scattered mode (BSE) and cathodoluminescence (CL) mode of scanning electron microscope (SEM). The trace element variation in topaz phenocrysts was studied in situ by electron probe microanalyser (EPMA) and laser ablation ICP-MS. Part of the sample has been crushed in a steel mortar and sieved. Quartz and topaz grains were hand-picked from the fraction 0.2 – 1 mm, mounted in epoxy and polished for inspection. Grains selected for melt inclusion studies were extracted from the epoxy using a hot needle and mounted individually. Previous studies have shown the high volatile content of quartz-hosted melt inclusions in these rocks (up to 12 wt.% H_2O; Naumov et al., 1984). During heating experiments, high water contents make quenching to homogeneous glass difficult, and boiling effects are commonly observed upon cooling (Naumov et al., 1971). Thus, we decided to study unheated melt inclusions. Unexposed and exposed melt inclusions were studied by laser Raman soectroscopy, EPMA, energy dispersion spectroscopy (SEM-EDS), and proton-induced X-ray emission microprobe (micro-PIXE).

EPMA and EDS

EPMA analyses of topaz phenocrysts, feldspar, mica and melt inclusion glass were carried out with a four WDS spectrometer-equipped Cameca SX100 electron microprobe at the Spectrum Centre of the University of Johannesburg. Beam intensity of 10 nA, acceleration of 10 kV and defocused beam (10 µm spot size) were used in order to prevent element diffusion. A set of natural minerals, including fluorite, Na-pyroxene, olivine, almandine, diopside, K-feldspar, wollastonite, halite, apatite, hematite and rutile, were used as reference materials. Elements were analysed for 10 to 30 s on-peak and off-peak. Detection limit, estimated from counting statistics, was between 200 and 500 ppm for most elements, except Fe (800 ppm) and F (1000 ppm). Additional analyses of glass and mineral phases were performed by EDS using a Tescan Vega 3 electron microscope equipped with a (Li)Si X-ray detector at the Spectrum Centre. Element calibration was made on a series of minerals and native elements. Spot size was 2 – 10 µm, acceleration 20 kV.

LA-ICP-MS

Trace element compositions of topaz phenocrysts have been investigated using laser ablation inductively-coupled mass spectrometry (LA-ICP-MS) at the University of Tasmania. A Coherent CompEX solid state 193 nm laser, and an Agilent 7500 quadrupole mass spectrometer were used. Analyses were performed along lines placed across growth textures identified by CL images, and into the groundmass. During the analyses, 20 seconds of background acquisition were followed by 100 s ablation at 3 µm/s speed, corresponding to traverses ~300 µm long. Ablation was performed at 10 Hz repetition rate, 30 µm spot size and 3.5 J/cm^2 fluence. Quantification of element concentrations was obtained using glass NIST 612 as primary standard and assuming stoichiometric abundance of Al, which was used as the internal standard. Glasses GSD1g and BCR were used as secondary standards.

Raman

In situ, non-destructive Raman analyses of multi-phase melt inclusions and various minerals were performed with a confocal laser Raman microscope (WITec alpha300R) at the Department of Geology, University of Johannesburg. The spectral range of the spectrometer is 100–4400 cm^{-1}. Raman spectra were collected using 20 X and 100 X Nikon objectives and a frequency doubled Nd:YAG (532 nm) Ar-ion 20-mW monochromatic laser source. Beam centring and Raman spectra calibration were performed daily before spectral acquisition using a Si standard (111). The optimum laser power for analyses of different minerals was determined experimentally. Raman spectra were compared with reference spectra from the RRUFF Database (Downs, 2006), and spectra from the literature. Additional Raman analyses were carried out at the central Laboratory of the University of Tasmania using a Renishaw inVia Raman microscope with Streamline.

PIXE-PIGE

Grains selected for proton-induced X-ray emission (PIXE) analysis were ground using sand paper and polishing powders until the inclusions were brought close to the surface (5 – 15 μm), polished and carbon-coated. PIXE allows analysis of unexposed inclusions, and quantification of the total composition of multiple phases, including fluids (e.g. Kamenetsky et al., 2002). PIXE microprobe analyses were performed on the nuclear microprobe at Materials Research Department of iThemba LABS, Somerset West, South Africa (Prozesky et al., 1995). This technology uses a very high-energy proton beam (3 MeV), focussed to a diameter of few micrometers, to excite the elements in a sample to emit characteristic X-rays and gamma-rays. PIXE microprobe analyses can provide both element concentration maps and bulk inclusion compositions, the process is non-destructive, can be used on unexposed inclusions, and requires no internal standard (Ryan et al., 2001). Fluorine was detected using proton-induced gamma-ray emission (PIGE).

4. Sample description

4.1 Mineral textures and compositions

Sample AB1 is a porphyritic rock with phenocrysts of quartz, K-feldspar, Na-plagioclase, topaz and mica (Fig 1A) embedded in quartz-feldspar-topaz groundmass. Phenocrysts are up to 2-3 mm across and represent ca. 30 vol.% of the rock. All minerals are very fresh, feldspar and topaz are water-clear and lack any sericite alteration. Quartz phenocrysts are brown to the naked eye (smoky quartz); under the microscope, they are subhedral to euhedral, and include feldspar. Subhedral to euhedral K-feldspar (sanidine Or56-73 Ab27-43), a few mm across, includes Na-plagioclase and mica. Plagioclase (Ab88-98 Or2-12) occurs as subhedral to euhedral crystals, ≤0.5 mm across and rimmed by K-feldspar, exhibiting polysynthetic Ab twinning. Topaz forms euhedral, prismatic and locally splinter-shaped phenocrysts up to 1-2 mm long. Topaz phenocrysts contain abundant mineral inclusions of Na-plagioclase, K-feldspar, aggregates of radially-oriented skeletal Nb-Ta-W oxide (W-ixiolite to tantalite-columbite), mica, round grains of quartz, and elongate to irregular grains of a Na-Al-F-phase (Fig 1B) identified as cryolithionite [$Na_3Li_3Al_2F_{12}$] by Raman peaks at ~567, 356 and 358 cm^{-1}. Raman spectroscopy of topaz showed the presence of a peak at ~3653 cm^{-1}, corresponding to the OH stretching vibration (Supplem Fig 1A).

Iron-bearing pleochroic dark brown-yellow mica with average Si/Al ~1.6 (zinnwaldite) forms subhedral to anhedral, ≤1-2 mm-long flakes (Fig 1C). Mica includes interleaved fluorite, and needles of Nb-Ta-W-oxide. Mica and topaz crystallised broadly at the same stage. This mica is a member of the siderophyllite [$KFe_2Al(Al_2Si_2O_{10})(F,OH)_2$] – polylithionite [$KLi_2Al(Si_4O_{10})(F,OH)_2$] series. It is zoned, and has pale green-yellow, BSE-darker rims, which have higher F (≤9.5 wt.%) and lower Fe concentrations (FeO ≤15.2 wt.%) compared to the brown-yellow, BSE-brighter cores (F = 5.9 – 7.6 wt.%, FeO = 15.9 – 21.5 wt.%). Recalculation of EPMA analyses on the basis of 11 oxygens indicates that F occupies 1.4 to 1.9 of the 2 hydroxyl sites, with the highest values in the rim suggesting crystallisation from a melt with increasing F/OH. The sum of cations accounts for 5.8 to 6.6 apfu of the 8 sites, and decreases towards the rim, suggesting a rimwards increase of Li content, which is not detected by EPMA.

Niobium-Ta-(W) oxide (W-ixiolite to columbite-tantalite) is particularly common as inclusions in topaz and mica phenocrysts; it also occurs in the groundmass, and was not identified in quartz and feldspar phenocrysts. Niobium-Ta-W oxide forms whisker-shaped or radial aggregates of brown needles, up to 200 μm long (Fig 1D), which do not show any particular distribution or orientation in host minerals. They contain 0 – 26. 8 wt.% W, 4.1 – 43.5 wt.% Nb, and appreciable amounts of Mn (≤7.4 wt.%). In a few grains, Sn was detected in high amounts (up to

49.3 wt.%), indicating the presence of cassiterite as inclusions, or possibly as an end-member component (Ercit, 1994). The groundmass is mainly composed of quartz, Na-plagioclase, K-feldspar and topaz (Fig 1E), and contains minor amounts of mica, zircon and monazite. Calcium-carbonate is present in irregular-shaped, texturally-late pockets in the groundmass, including a fine-grained Al-Si mineral (dickite or kaolinite), and locally fluorite (Fig 1F), zircon and W-ixiolite. Fluorite occurs in two generations: 1) early fluorite I forms eu- subhedral crystals in the groundmass and inclusions in quartz phenocrysts in contact with silicate melt, and contains REE and Y in amounts detectable by EDS; 2) fluorite II is late, it occurs as veinlets and anhedral grains in the groundmass and is trace element-poor.

4.2 CL of topaz and quartz phenocrysts

CL has been used to reveal the crystal habit of the phenocrysts at different stages of growth (growth textures) and post-crystallisation deformation features (secondary textures, e.g. Watt et al., 1997). In topaz phenocrysts, CL variations define euhedral to lobed growth textures. In several cases, CL-bright zones are followed by truncation of growth textures, suggesting resorption events (Fig 2A). The most prominent feature in CL images is represented by a rim, several hundred µm wide (Fig 2B). This rim, particularly well-developed on pyramidal facets rather than prisms, represents a late overgrowth and is separated by crystal cores by a rounded surface truncating growth textures. In several grains, a very CL-bright discontinuous layer of topaz immediately follows the truncation contact (Fig 2B, 2C). Abundant round quartz inclusions are trapped in this overgrowth (Fig 2B and inset). Round quartz inclusions are up to few tens of µm across, and distributed in narrow bands parallel to the topaz grain margins. EPMA indicates that round quartz inclusions have Al_2O_3 up to 0.56 wt.%.

Quartz phenocrysts show complex CL patterns, most of which cannot be correlated between different grains. CL of quartz grains shows both continuous variations and abrupt changes of brightness (step zones). Several step zones can be present in single crystals, and some of these mark truncations of euhedral growth textures (Fig 2D). Truncation of CL zones occurs mostly as rounding of crystal corners, and as wavy contacts cross-cutting growth textures (Fig 2E). Thin oscillatory zones (up to 20 – 30 µm wide) within super-ordinate stepped zones are mostly parallel to stepped zones (Fig 2D, 2E). Sector-zoning is present in many grains (Fig 2D).

Round healed cracks, filled with recrystallized quartz, are present in most quartz phenocrysts and do not cross-cut the surrounding groundmass. Quartz in these cracks appears as either CL-darker, or CL-brighter than the surrounding quartz, and significant brightness changes are observed even along the same crack (Fig 2D, 2E).

5. Topaz- and quartz-hosted melt inclusions

5.1 Topaz-hosted inclusions

Topaz-hosted melt inclusions are elongate to irregular-shaped, up to 70 – 80 µm in size. Some of these melt inclusions occur as clusters of numerous inclusions oriented along planes (Fig 3A). In other cases, the inclusions are isolated, locally co-trapped with minerals (W-ixiolite, feldspar) (Fig 3B). Textural relationships suggest equilibrium between W-ixiolite and this melt. Topaz-hosted melt inclusions contain colourless glass, a bubble and, in many cases, an anhedral colourless/pale pink phase (cryolithionite). This latter colourless phase displays a variety of forms, from round and irregular (Fig 3A insets) to cubic (Fig 3B), and may have originally formed either as crystals or possibly as an immiscible melt. An aggregate of fine-grained crystals in some isolated melt inclusions was identified as mica by EDS analysis. A few 2-phase inclusions, containing a H_2O-rich bubble surrounded by clear glass, were found along a plane associated with glass-vapour-crystal-bearing inclusions. Raman spectra of glass in topaz-hosted melt inclusions was hindered by high fluorescence, but locally showed a broad peak at 3200 – 3500 cm^{-1} (Supplem Fig 1C), indicative of the vibrational modes of water (Walrafen, 1964). Bubbles did not give any Raman spectra. Some topaz-hosted inclusions consist of irregular, elongated and up to 300 µm-long aggregates of fine-grained minerals, mostly K-feldspar, albite and mica, conferring a semi-opaque appearance to these inclusions.

5.2 Quartz-hosted inclusions

Quartz-hosted melt inclusions occur both in the core and the rim of the phenocrysts. They tend to show a subhedral negative crystal shape, and are up to 100 µm in size. These inclusions contain clear (colourless-pale pink) to semi-opaque glass, a bubble (typically < 10 vol.% of the inclusions), and locally crystals (Fig 3C). Some crystals in these melt inclusions are colourless and sub- to anhedral, others are colourless and cubic, or yellow. Some of these colourless grains were identified as fluorite by Raman spectroscopy. Very fine-grained precipitates, and dendritic crystals have nucleated on some bubbles. Locally, quartz-hosted melt inclusions also contain an elongate prismatic crystal of apatite, identified by a peak at 964 cm^{-1} in the Raman spectrum (Frezzotti et al., 2012). Some quartz crystals contain tube-like melt inclusions, several hundreds of µm long and around 10 µm wide. Such inclusions, composed of glass and a vapour bubble, have "dusty" appearance due to very fine-grained crystals, similar to what has been described in topaz in pegmatite from the Kymi topaz-granite (Lukkari et al., 2009). Round and homogeneous (single-phase) vapour inclusions are spatially associated with these inclusions. Separation of glass (melt) and vapour (homogeneous inclusions) may have been due to annealing processes (necking down). In addition, very irregular melt inclusions were observed in some quartz grains. These contain clear, colourless glass, a bubble, and occasionally a small opaque crystal, likely a daughter phase (Fig 3D), and a colourless crystal (mica). These inclusions are spatially related with cracks appearing on the grain surface and with small fluid inclusions. The cracks possibly represent fractures along which melt was injected, thus implying a secondary origin of the melt inclusions.

Raman spectra of glass in quartz-hosted inclusions have high background, and locally show a broad Raman peak between ~3200 and 3500 cm^{-1}, indicating the presence of water. In some subhedral inclusions, co-occurrence of Raman peaks at 1080 cm^{-1} and the diamond-graphite peaks (~1335 and 1608 cm^{-1}) indicate presence of carbonate ion dissolved in the glass (Thomas et al., 2009; Amalberti et al., 2012). The bubbles did not give any Raman response, thus suggesting these are shrinkage voids. Round fluorite crystals, up to 50 – 60 µm in size, surrounded by a thin film (up to 5 µm) of silicate glass were found in some quartz grains (Fig 3E). Raman analysis of these fluorite grains show characteristic spectra with broad and very intense peaks (Supplem Fig 1D), and EDS indicates the presence of Y and Ce (Fig 3E).

5.3 Melt inclusion analyses (EDS, EPMA, PIXE)

The composition of glass in melt inclusions is characterised by SiO_2 = 62 – 76 wt.%, K_2O = 3.5 – 7.0, Na_2O = 2.8 – 6.0 wt.% (all recalculated to 100 % anhydrous) (Fig 4, Table 1). Contents of FeO, MgO and CaO are very low in all analyses (<0.3, <0.1 and <0.5 wt.%, respectively); Cl concentrations are up to 0.4 wt.%. Fluorine contents vary substantially, ranging from below detection limit to 9.3 wt.%. The highest F values were measured in irregular-shaped (secondary?) inclusions in topaz and quartz, whereas sub-euhedral quartz-hosted melt inclusions have F ≤1.2 wt.% (Fig 4). All melt inclusions are peraluminous, with alumina saturation index (ASI = $Al_2O_3/(Na_2O + K_2O + CaO)$, molar) increasing from 1.18 and 1.89 with increasing SiO_2. The irregular-shaped melt inclusions have decreasing F and Na_2O with increasing SiO_2, and have higher ASI and K_2O at similar SiO_2 in comparison with subhedral quartz-hosted inclusions. The presence of Cs (up to 0.47 wt.%) was observed by EDS in some topaz-hosted melt inclusions.

In PIXE maps of topaz-hosted inclusions, K, Rb, Cs and As are distributed in the glass, whereas (daughter?) mineral phases are characterised by co-occurring peaks of Fe, Mn and Ca, and peaks of Cu and Zn (Fig 5A). Potassium, Fe, Mn, Ca, Rb, Zn, Cu, Ge and As were detected in topaz-hosted opaque (crystallised) inclusions by PIXE. In PIXE maps of subhedral quartz-hosted inclusions, K, Rb, Zr, Nb, F (measured by PIGE), Fe, ±Ca, ±Mn, ±As, ±Ga, ±Pb are associated with the glass. Minerals in these inclusions are shown by intense peaks of Fe and Mn co-occurring with Zn in some maps, possibly indicating oxide or mica (Fig 5B). No elements were detected in bubbles during PIXE analyses, although fine-grained opaque precipitates on some bubbles, gave Fe, Mn, Cu, Ti and Ca peaks. PIXE maps of irregular quartz-hosted inclusions detected K, Rb, As, F, Fe, Nb, Pb in the glass (Fig 5C).

6. Topaz micro-chemical characterisation

EPMA

Major element composition of topaz phenocrysts has been analysed along core-to-rim traverses to estimate the F content, and to calculate the amount of OH replacement. All the analyses indicate high contents of F (20.6 – 22.2 wt.%). The rims, as defined by CL images, are slightly F-richer than the cores (F ≥21.8 wt.%, Fig 6). Small amounts of P (up to 0.1 wt.%) were measured in the cores, and analyses with P above detection limit (200 ppm) have broad negative correlation with Si. Recalculations based on two Al atoms indicate slight Si deficiency (Si = 0.97 – 0.99 apfu) and slight F excess, even in the cores (cores F = 2.03 – 2.16, rims F = 2.10 – 2.17 apfu). Totals are between 97.5 and 100.4 wt.% for the cores and 99.1 and 100.3 wt.% for the rims, and have a broad positive correlation with F (Fig 6, Table 2). Although the recalculations suggest total saturation of the OH site by F, totals smaller than 100 wt.% allow the presence of a small amount of water in topaz (OH/(OH+F)

≤0.09). Presence of water in topaz is also indicated by an OH stretching peak at ~3653 cm^{-1} in Raman spectra (Supplem Fig 1A). Fluorine contents do not show correlations with CL intensity.

LA-ICP-MS

Trace element traverses of topaz phenocrysts have been analysed across the core-rim boundary. Plots of the signal intensity (as counts per second, cps) versus ablation time (and distance) indicate strong variations corresponding to the core-rim boundary. Across this boundary, Li signal intensity increases by one order of magnitude or more (Fig 7). Quantification of analyses indicates that the cores contain Li from <1.2 to 35 ppm, whereas the rims contain 62 – 130 ppm Li. Signal intensities of Nb, Ta, W and Sn also increase significantly (around one order of magnitude) across the same boundary. Recalculations indicate that the rims contain 1.1 – 36 ppm Ta, 6.8 – 80 ppm W and 2.6 – 125 ppm Nb (Fig 8, Table 3). Boron and Be, mostly below detection limit in the cores (i.e., <4 and 1.5 ppm, respectively), also increase in the rims, which have B ≤11 ppm and Be 3.2 – 17 ppm. On average, the rims are enriched compared to the cores, in most lithophile elements (light REE, Y, Rb, Sr, Cs, Zr, Mn, K, Na, Th, U) by factors varying between 10 (Sn) and 500 (Mn), although no clear variation was found in Pb, Ca, Cu and Zn, and only marginal increase in Ga, Fe, P and Sc. In contrast with the core-rim boundary, trace element concentrations in the cores have moderate and smooth variations corresponding to CL changes, some of which suggest truncation and resorption. Gallium, Li, W, Nb and Ta to a different extent, appear to be enriched in CL-brighter areas (Fig 7B). The lack of spikes in time-resolved LA-ICP-MS signal plots suggests that trace element analyses were not affected by inclusions.

7. Discussion

7.1 Implications of CL textures and trace element compositions of topaz

Multiple resorption events, implied by truncations of CL textures in topaz as well as quartz, suggest a very dynamic environment with frequent shifts from saturation to undersaturation. Topaz in magmatic rocks tends to have lower OH/(OH+F) than metamorphic topaz. OH/(OH+F) replacement up to 0.3 (F 1.4, OH 0.6 apfu) has been reported in hydrothermal deposits (Barton, 1982), and OH/(OH+F) = 0.35 – 0.55 has been reported from the ultra-high pressure metamorphic Sulu terrane, China (Zhang et al., 2002), whereas topaz from granite in the Krušné Hory/Erzgebirge area has OH/(OH+F) ~ 0.05 (or OH = 0.1 apfu) (Breiter et al., 2013). Fluorine content in magmatic topaz has been shown to be temperature-dependent (Thomas, 1982). Despite the presence of OH, as detected by Raman spectroscopy, the near-pure composition of topaz [$Al_2SiO_4F_2$] measured in this study (OH/(OH+F) $\leq$0.09) is consistent with a magmatic origin.

Concentrations of Li and B in the rims of topaz phenocrysts presented in this study are comparable to the concentrations analysed by Hervig et al. (1987) in topaz from rhyolites of the North American Cordillera. Locally high concentrations of P (up to 1 wt.%), and Fe (31 – 1296 ppm), Ge (26 – 104 ppm), Sc (2 – 12 ppm), Sn (1 – 30 ppm) and Ga (2 – 29 ppm) were measured in topaz from granites in the Krušné Hory/Erzgebirge area (Breiter et al., 2013). Vanadium (occurring as V^{4+}), Mn (as Mn^{3+}), Ti (as Ti^{4+}), Cr (as Cr^{3+}) at tens to hundreds of ppm levels have been detected by EPMA and electric paramagnetic resonance (EPR) in gem-quality topaz from Ouro Preto, Brazil (Schott et al., 2003). Further, a large number of elements was analysed by K_0-INAA in topaz from Pakistan, including Mn, Fe and Na at hundreds to tens of thousands ppm levels, As, Br, light REE, Co, Cr, Cs, Ga, Ge, Hf, Rb, Sb, Sc, Th, U, Zn at ppm to tens of ppm levels, and Ta, W and HREE, mostly at sub-ppm levels (Wasim et al., 2011), although these authors do not specify the origin of these topaz crystals.

Indications on the nature of trace element incorporation in topaz can be obtained from the chemical analyses. The smooth time-resolved LA-ICP-MS signals (Fig 7) suggest that trace elements are incorporated in the mineral lattice, rather than in discrete inclusions, although the presence of nanoinclusions smaller than the resolution power of this technique cannot be ruled out. In the peraluminous granites and greisens in the Podlesı granite, replacement of (Si + Si) by (P + Al) has been proposed (Breiter et al., 2013). A weak negative P – Si correlation in our EPM analyses seems to indicate the same type of substitution (Fig 6B). Based on simple charge balance considerations, replacement of Si by other cations in the 4+ oxidation state (e.g. Ti, V), and replacement of Al^{3+} by 3+ cations (Ga, Fe, Mn) seem plausible. Intake of Nb, Ta and W, which usually occur in the 5+ oxidation state, would require coupled substitution.

Although the CL properties of topaz and the nature of the CL "activator" elements are largely unknown (MacRae and Wilson, 2008), it is likely that the intake of impurities, with consequent distortion of the mineral lattice, may be responsible for increase of CL intensity of topaz. This hypothesis is supported by the correlation between Nb, Ta, W, Li and Ga with CL intensity in our samples (Fig 7). The replacement of OH for F is known to affect the cell parameters of topaz (Alberico et al., 2003; Schott et al., 2003; Zhang et al., 2002), thus potentially affecting the luminescence properties. However, although the trace element-enriched, CL-bright rims have higher F contents than the cores, no clear correlation was found between F content in EPM analyses and CL intensity in the samples we studied.

7.2 Melt evolution

Melt inclusion textures and compositions indicate the presence of two silicate melts. One melt is recorded by subhedral inclusions hosted in quartz and the second by irregular-shaped inclusions hosted in both topaz and quartz. The wide variations of F (up to 9.3 wt.%) and the negative correlation of F with SiO_2 in topaz-hosted and irregular-shaped quartz-hosted melt inclusions (Fig 4) can be modelled by fractionating variable proportions of a phase with a composition similar to cryolithionite from the lowest SiO_2, highest F compositions. An anhedral phase with cryolithionite composition has been observed in melt inclusions (Fig 3A, 3B), and elongate grains of the same phase were also found in topaz (Fig 1B). Thus, separation of this phase may have occurred after melt entrapment (as a daughter phase), or prior to entrapment during topaz crystallisation. Cryolithionite may have formed as an immiscible liquid, as suggested by the anhedral habit of these grains. The presence of a Na-Al-F glass in the Ary-Bulak massif was identified by EDS analysis by Peretyazhko and Savina (2010b), who interpreted it as deriving from an immiscible fluoride liquid. The decrease in Na_2O and Al_2O_3, as well the increase of ASI with increasing SiO_2, can also be explained by separation of a cryolithionite-like phase. Conversely, K_2O, which shows a mild decrease with increasing SiO_2 (Fig 4), cannot be satisfactorily modelled by simple cryolithionite fractionation. This mismatch may be explained by crystallisation of other K-bearing phases, such as mica, which formed together with topaz. Thus, the highest F values measured are more indicative of the melt composition at the moment of trapping. Topaz likely crystallised from such F-enriched melt.

Previous studies of quartz-hosted melt inclusions have measured F contents higher than in the subhedral melt inclusions, but similar to the irregular, late-trapped inclusions considered in this study. Antipin et al. (2009) and Kuznetsov et al. (2004) measured up to 6.2 wt.% F, Peretyazhko and Savina (2010a) up to 7.8 wt.% F, calculated on an anhydrous basis. These authors described quartz-hosted melt inclusions as occurring exclusively at the rim of quartz phenocrysts, thus suggesting trapping at a relatively late stage of magma evolution. In contrast, subhedral quartz-hosted melt inclusions analysed here, which occur throughout the host minerals and contain F $\leq$1.2 wt.%, may be representative of an earlier stage of melt evolution.

Thus, comparison of early- and late-trapped melt inclusions indicates a strong increase in the F content of the melt. Further, separation of cryolithionite from the topaz-hosted melt indicates high concentrations of Li. Cryolithionite (which contains ~60 wt.% F, ~18 wt.% Na and 5.6 wt.% Li by stoichiometry) constitutes ~2 – 3 vol.% of the inclusions, contributing ~1100 – 1700 ppm Li to the composition of the whole inclusion. The rims of topaz phenocrysts and mica also show an increase in F, as well as Li, compatible with the F increase recorded by melt inclusions. Both early and late melts are peraluminous, in agreement with the mineralogy of the rock (including mica and topaz). The relation between the two melts is not clear. For example, the measured F increase (~1 to 9 wt.%) is difficult to explain by fractionation of the modal minerals. Even assuming a completely incompatible behaviour of F (which is inconsistent with petrographic observations), such increase would imply crystallisation of almost 90 % of the melt, which is in contrast with the phenocryst abundance in these rocks (up to 20 – 30 %). However, the F-rich melt could have developed in pockets of residual melt, similar to miaroles, frequently observed in shallow intrusions, and later remobilised. Feldspar-mica-quartz crystallised inclusions in topaz phenocrysts likely indicate that part of the groundmass was crystallised when the topaz phenocrysts formed, and are in agreement with this hypothesis.

The occurrence of some melt inclusions along cracks suggests a very low viscosity of the trapped liquid. Such low viscosity can be explained by considering the strong viscosity-reducing effect of F (Giordano et al., 2008). According to the model proposed by these authors, addition of 9 wt.% F would cause a decrease of ln(η) of a rhyolitic melt (SiO_2 = 70 wt.%, K_2O = Na_2O = 5 wt.%) by ~5 log units at 800°C (from ln(η)~$10^{10.3}$ to $10^{5.5}$ Pa·s) and 7.8 log units at 600°C (from ln(η)~$10^{15.8}$ to $10^{8.0}$

Pa·s), and any water present would further decrease viscosity in a similar way to F. Such extremely low viscosity would favour the separation of this melt from the crystals and its migration towards the margins of intrusions and into the country rocks, and may result in wall-rock alteration and mineralisation processes described around F-rich intrusions, such as veining and greisenisation, which in many cases contain large amounts of Nb-Ta-W minerals (Badanina et al., 2006; Charoy and Noronha, 1996; Kinnaird, 1985; Melcher et al., 2014).

7.3 Saturation of Nb-Ta-W-(Sn) in the melt and implications for mineralisation

The close association of Nb-Ta-(W) oxide with topaz was previously observed in the Ary-Bulak massif (Kovalenko and Kovalenko, 1976; Peretyazhko and Savina, 2010b), and in topaz granite dykes of the Totoguz massif (Letnikov, 2008), which is compositionally similar to ongonites. We observed needles of Nb-Ta-(W) oxide in late-crystallising topaz, but not in quartz or feldspar, which suggests a link between concentrations of these elements during the late stages of magma fractionation and the formation of topaz. Niobium-Ta-W-(Sn) oxides showing no signs of disequilibrium (e.g. resorption) were found in direct contact with topaz-hosted melt inclusions (Fig 3B), and were therefore likely in equilibrium with this F-(Li)-rich peraluminous melt.

Experiments have demonstrated a strong increase of Nb, Ta and W solubility in felsic melts with increasing F (Keppler, 1993), Li (Bartels et al., 2010; Linnen, 1998) and alkali content (Linnen and Keppler, 1997). Thus, the increase of F and Li in the melt – indicated by melt inclusions and growth zones of topaz and mica – would cause incompatible behaviour of Nb, Ta and W, and promote their concentration in the melt with progressive crystallisation. Subsequently, separation of a cryolithionite-like phase (Fig 1B, 3A) would deplete the melt in F, Li and alkalis, thus reducing the solubility of Nb, Ta and W, and causing precipitation of W-ixiolite and tantalite-columbite (Fig 9). Textures of Nb-Ta-(W) oxides, such as needle-like crystals arranged in radial aggregates, suggest rapid crystallisation under conditions of strong oversaturation, implying marked F and Li depletion. These processes are recorded in topaz chemical zones and CL properties, which indicate repeated variations of luminescence associated with fluctuations of trace element contents (including Nb, Ta, W and Li). In some cases, CL-bright, Nb-Ta-W-Li-enriched growth zones of topaz are followed by a resorption event (Fig 2A, 2B). This seems to indicate periodic accumulation of these elements in the melt, followed by resorption and successive growth of CL-darker, Nb-Ta-W-poorer topaz. Topaz destabilisation may have occurred following strong F depletion due to cryolithionite separation.

8. Conclusions

The detailed textural and microchemical study of topaz and the analyses of melt inclusions hosted in quartz and topaz phenocrysts from the Ary-Bulak ongonite massif, Russia, offer insight into the formation of magmatic topaz. EPM analyses indicate that topaz in these rocks is composed of an almost pure F component containing an average of ~21 wt.% F, and OH/(OH + F) ≤0.09 (calculated by difference, 100 wt.% – EPMA tot). LA-ICP-MS revealed the presence of a large number of trace elements, including Fe, Na, P, Li, B, Be, Nb, Ta, W, Ga, Ba, REE. The concentrations of some of these elements (Li, Ga, Nb, Ta, W) are co-varying with cathodoluminescence intensity, suggesting a role of some of these elements as CL-activators in topaz. Variations of CL intensity and trace element contents of topaz may be used as a proxy for Nb-Ta-W fluctuations in the melt. Early-trapped, quartz-hosted subhedral melt inclusions are mildly peraluminous (ASI = 1.2 on average) and contain F ~1 wt.%. Topaz-hosted melt inclusions indicate that topaz crystallised from a strongly F-enriched (up to >9 wt.%), peraluminous, low-Ca melt, and contain cryolithionite [$Na_3Li_3Al_2F_{12}$] as a daughter phase. Topaz and Nb-Ta-W-oxide crystallised from this F-Li-enriched melt. The high F and Li contents would have favoured the concentration of high-field strength elements during magmatic processes, so that this melt became enriched in Nb, Ta and W. Subsequent separation of a cryolithionite-like phase (as either an immiscible melt or a crystalline phase) would have caused a drop in F and Li, reduced the solubility of high-field strength elements, and promoted crystallisation of tantalite-columbite and W-ixiolite. This melt had an extremely low viscosity and was thus highly mobile, as demonstrated by the occurrence of melt inclusions along cracks. Such a melt would have the capability to escape crystallising intrusions and domes, and may have a role in the formation of greisens and mineralised topaz-bearing veins around felsic intrusions of similar composition to the Ary-Bulak massif.

Acknowledgments

This research was made possible to a Post-Doctoral Fellowship of the National Research Foundation of South Africa and a University of Tasmania Visiting Scholar

Fellowship to AA. Thomas Rodemann (University of Tasmania), Jay Thompson (CODES, University of Tasmania) and Christian Reinke (University of Johannesburg) are thanked for their assistance with the Raman, LA-ICP-MS and EPMA. Vladimir Naumov and Reiner Thomas are thanked for their constructive comments.

References

Alberico, A., Ferrando, S., Ivaldi, G., Ferraris, G., 2003. X-ray single-crystal structure refinement of an OH-rich topaz from Sulu UHP terrane (Eastern China) – Structural foundation of the correlation between cell parameters and fluorine content. European Journal of Mineralogy 15, 875-881.

Amalberti, J., Neuville, D.R., Sarda, P., Sator, N., Guillot, B., 2012. Quantification of CO_2 dissolved in silicate glasses and melts using Raman spectroscopy: implications for geodynamics. Mineralogical Magazine 76, 430.

Antipin, V.S., Andreeva, I.A., Kovalenko, V.I., Kuznetsov, V.A., 2009. Geochemical specifics of ongonites in the Ary-Bulak Massif, eastern Transbaikalia. Petrology 17, 558-569.

Antipin, V.S., Savina, E.A., Mitichkin, M.A., 2006. Geochemistry and formation conditions of rare-metal granites with various fluorine-bearing minerals (fluorite, topaz, and cryolite). Geochemistry International 44, 965-975.

Badanina, E., Trumbull, R.B., Dulski, P., Wiedenbeck, M., Veksler, I.V., Syritso, L.F., 2006. The behaviour of rare-earth and lithophile trace elements in rare-metal granites: a study of fluorite, melt inclusions and host rocks from the Khangilay complex, Transbaikalia, Russia. The Canadian Mineralogist 44, 667-692.

Bartels, A., Holtz, F., Linnen, R.L., 2010. Solubility of manganotantalite and manganocolumbite in pegmatitic melts. American Mineralogist 95, 537-544.

Barton, M.D., 1982. The thermodynamic properties of topaz solid solutions and some petrologic applications. American Mineralogist 67, 956-974.

Breiter, K., Gardenová, N., Vaculovič, T., Kanický, V., 2013. Topaz as an important host for Ge in granites and greisens. Mineralogical Magazine 77, 403-417.

Burt, D.M., Sheridan, M.F., Bikun, J.V., Christiansen, E.H., 1982. Topaz rhyolites; distribution, origin, and significance for exploration. Economic Geology 77, 1818-1836.

Charoy, B., Noronha, F., 1996. Multistage growth of a rare-element, volatile-rich microgranite at argemela (Portugal). Journal of Petrology 37, 73-94.

Christiansen, E.H., Bikun, J.V., Sheridan, M.F., Burt, D.M., 1984. Geochemical evolution of topaz rhyolites from the Thomas Range and Spor Mountain, Utah. American Mineralogist 69, 223-236.

Christiansen, E.H., Burt, D.M., Sheridan, M.F., Wilson, R.T., 1983. The petrogenesis of topaz rhyolites from the western United States. Contributions to Mineralogy and Petrology 83, 16-30.

Christiansen, E.H., Lee, D.E., 1986. Fluorine and chlorine in granitoids from the Basin and Range Province, Western United States. Economic Geology 81, 1484-1494.

Congdon, R.D., Nash, W.P., 1988. High-fluorine rhyolite: An eruptive pegmatite magma at the Honeycomb Hills, Utah. Geology 16, 1018-1021.

Dolejš, D., Baker, D.R., 2007. Liquidus equilibria in the system K2O-Na2O-Al_2O_3-SiO_2-F_2O_{-1}-H_2O to 100 MPa: II. Differentiation paths of fluorosilicic magmas in hydrous systems. Journal of Petrology 48, 807-828.

Downs, R.T., 2006. The RRUFF Project: an integrated study of the chemistry, crystallography, Raman and infrared spectroscopy of minerals. Program and Abstracts of the 19th General Meeting of the International Mineralogical Association in Kobe, Japan. O03-13.

Ercit, T.S., 1994. The geochemistry and crystal chemistry of columbite-group minerals from granitic pegmatites, southwestern Grenville Province, Canadian Shield. The Canadian Mineralogist 32, 421-438.

Frezzotti, M.L., Tecce, F., Casagli, A., 2012. Raman spectroscopy for fluid inclusion analysis. Journal of Geochemical Exploration 112, 1-20.

Gioncada, A., Orlandi, P., Vezzoli, L., Omarini, R.H., Mazzuoli, R., Lopez-Azarevich, V., Sureda, R., Azarevich, M., Acocella, V., Ruch, J., 2014. Topaz magmatic crystallization in rhyolites of the Central Andes (Chivinar volcanic complex, NW Argentina): Constraints from texture, mineralogy and rock chemistry. Lithos 184–187, 62-73.

Giordano, D., Russell, J.K., Dingwell, D.B., 2008. Viscosity of magmatic liquids: A model. Earth and Planetary Science Letters 271, 123-134.

Haapala, I., 1977. Petrography and geochemistry of the Eurajoki stock; a rapakivi-granite complex with greisen-type mineralizationin southwestern Finland. Geological Survey of Finland Bulletin 286, 1-128.

Haapala, I., 1997. Magmatic and postmagmatic processes in tin-mineralized granites: topaz-bearing leucogranite in the Eurajoki Rapakivi Granite Stock, Finland. Journal of Petrology 38, 1645-1659.

Haapala, I., Lukkari, S., 2005. Petrological and geochemical evolution of the Kymi stock, a topaz granite cupola within the Wiborg rapakivi batholith, Finland. Lithos 80, 347-362.

Haapala, I., Thomas, R., 2000. Melt inclusions in quartz and topaz of the topaz granite from Eurajoki, Finland. Journal of the Czech Geological Society 45, 149-154.

Hervig, R.L., Kortemeier, W.T., Burt, D.M., 1987. Ion-microprobe analyses of Li and B in topaz from different environments. American Mineralogist 72, 392-396.

Kamenetsky, V.S., van Achterbergh, E., Ryan, C.G., Naumov, V.B., Mernagh, T.P., Davidson, P., 2002. Extreme chemical heterogeneity of granite-derived hydrothermal fluids: An example from inclusions in a single crystal of miarolitic quartz. Geology 30, 459-462.

Keppler, H., 1993. Influence of fluorine on the enrichment of high field strength trace elements in granitic rocks. Contributions to Mineralogy and Petrology 114, 479-488.

Kinnaird, J.A., 1985. Hydrothermal alteration and mineralization of the alkaline anorogenic ring complexes of Nigeria. Journal of African Earth Sciences 3, 229–251.

Kortemeier, W.T., Burt, D.M., 1988. Ongonite and topazite dikes in the Flying W ranch area, Tonto basin, Arizona. American Mineralogist 73, 507-523.

Kostitsyn, Y.A., Kovalenko, V.I., Yarmolyuk, V.V., 1996. Rubidium-strontium isochron for the Arybulak ongonite stock, eastern Transbaikalia. Transactions (Doklady) of the Russian Academy of Sciences. Earth science sections.

Kovalenko, V.I., Grebennikov, A.M., Antipin, V.S., 1975. Ongonite of the Arybulak stock, Transbaikal: the first find of a subvolcanic analog of rare metal-bearing lithium-fluorine granite (apogranite) in the USSR. Doklady, Academy of Sciences of the USSR, Earth Sciences Section 220, 158-160.

Kovalenko, V.I., Kovalenko, N.I., 1976. Ongonites (topaz bearing quartz keratophyre)-subvolcanic analogue of rare metal Li-F granite. Nauka Press.

Kovalenko, V.I., Kuzmin, M.I., Antipin, V.S., Petrov, L.L., 1971. Topaz-bearing quartz keratophyre (ongonite), a new variety of subvolcanic igneous dike rocks. Doklady Akademii Nauk SSSR, Earth Science Section 199, 132-135.

Kovalenko, V.I. et al., 2007. Two types of magma sources of rare-metal alkali granites. Geology of Ore Deposits 49, 442-466.

Kuznetsov, V.A., Andreeva, I.A., Kovalenko, V.I., Antipin, V.S., Kononkova, N.N., 2004. Abundance of water and trace elements in the ongonite melt of the Ary-Bulak massif, Eastern Transbaikal Region: Evidence from study of melt inclusions. Doklady Earth Sciences 396, 571–576.

Letnikov, F.A., 2008. Topaz granites in northern Kazakhstan. Petrology 16, 319-334.

Linnen, R.L., 1998. The solubility of Nb-Ta-Zr-Hf-W in granitic melts with Li and Li + F; constraints for mineralization in rare metal granites and pegmatites. Economic Geology 93, 1013-1025.

Linnen, R.L., Keppler, H., 1997. Columbite solubility in granitic melts: consequences for the enrichment and fractionation of Nb and Ta in the Earth's crust. Contributions to Mineralogy and Petrology 128, 213-227.

Lukkari, S., 2002. Petrography and geochemistry of the topaz-bearing granite stocks in Artjärvi and Sääskjärvi, western margin of the Wiborg rapakivi granite batholith. Bulletin of the Geological Society of Finland 74, 115-132.

Lukkari, S., Holtz, F., 2007. Phase relations of a F-enriched peraluminous granite: An experimental study of the Kymi topaz granite stock, southern Finland. Contributions to Mineralogy and Petrology 153, 273-288.

Lukkari, S., Thomas, R., Haapala, I., 2009. Crystallization of the Kimi topaz granite stock within the Wiborg rapakivi granite Batholith, Finland: evidence from melt inclusions. The Canadian Mineralogist 47, 1359-1374.

MacRae, C.M., Wilson, N.C., 2008. Luminescence database I - Minerals and materials. Microscopy and Microanalysis 14, 184-204.

Melcher, F., Graupner, T., Gäbler, H.-E., Sitnikova, M., Henjes-Kunst, F., Oberthür, T., Gerdes, A., Dewaele, S., Tantalum–(niobium–tin) mineralisation in African pegmatites and rare metal granites: Constraints from Ta–Nb oxide mineralogy, geochemistry and U–Pb geochronology (in press). Ore Geology Reviews. http://dx.doi.org/10.1016/j.oregeorev.2013.09.003

Moghazi, A.M., Harbi, H.M., Ali, K.A., 2011. Geochemistry of the Late Neoproterozoic Hadb adh Dayheen ring complex, Central Arabian Shield: Implications for the origin of rare-metal-bearing post-orogenic A-type granites. Journal of Asian Earth Sciences 42, 1324-1340.

Naumov, V.B., Kovalenko, V.I., Clocchiatti, R., Solovova, I.P., 1984. Crystallization parameters and phase compositions for melt inclusions in ongorhyolite quartz. Geochemistry International 21, 19-31.

Naumov, V.B., Kovalenko, V.I., Kuz'min, M.I., Vladykin, N.V., Ivanov, G.V., 1971. Thermometric study of inclusions of melt in topaz from the topaz-bearing quartz keratophyre (ongonite). Doklady Akademii Nauk SSSR, Earth Science Section 199, 104-106.

Naumov, V.B., Solovova, I.P., Kovalenko, V.I., Guzhova, A.V., 1991. The crystallization of topaz, albite, potash feldspar, mica, and columbite from an ongonite magma. Geochemistry International 28, 120-124.

Peretyazhko, I.S., Savina, E.A., 2010a. Fluid and magmatic processes in the formation of the Ary-Bulak ongonite massif (eastern Transbaikalia). Russian Geology and Geophysics 51, 1110-1125.
Peretyazhko, I.S., Savina, E.A., 2010b. Sinks of liquid immiscibility in ongonitic magma: Evidence from the study of melt and fluid inclusions in rocks of the Ary-Bulak massif (Eastern Transbaikalia). Doklady Earth Sciences 433, 1077-1082.
Peretyazhko, I.S., Savina, E.A., Dril', S.I., Gerasimov, N.S., 2011. Rb–Sr isotope system and Rb–Sr partitioning in the rocks of the Ary-Bulak ongonite massif, formed with the participation of fluoride–silicate magmatic immiscibility. Russian Geology and Geophysics 52, 1401-1411.
Peretyazhko, I.S., Tsareva, E.A., Zagorsky, V.Y., 2007a. A first finding of anomalously Cs-rich aluminosilicate melts in ongonite: Evidence from melt inclusion study. Doklady Earth Sciences 413, 462-468.
Peretyazhko, I.S., Zagorsky, V.Y., Tsareva, E.A., Sapozhnikov, A.N., 2007b. Immiscibility of calcium fluoride and aluminosilicate melts in ongonite from the Ary-Bulak intrusion, Eastern Transbaikal region. Doklady Earth Sciences 413, 315-320.
Prozesky V.M., Przybyłowicz W.J., Van Achterbergh E., Churms C.L., Pineda C.A., Springhorn K.A., Pilcher J.V., Ryan C.G., Kritzinger J., Schmitt H., Swart T., 1995. The NAC nuclear microprobe facility. Nuclear Instruments and Methods in Physics Research B 104, 36-42.
Ryan, C.G., McInnes, B.I.A., Williams, P.J., Dong, G., Win, T.T., Yeats, C.J., 2001, Imaging fluid inclusion content using the new CSIRO-GEMOC nuclear microprobe. Nuclear Instruments and Methods in Physics Research Section B—Beam Interactions with Materials and Atoms 181, 570–577.
Schott, S., Rager, H., Schürmann, K., Taran, M., 2003. Spectroscopic study of natural gem quality "Imperial" topazes from Ouro Preto, Brazil. European Journal of Mineralogy 15, 701-706.
Štemprok, M., 1991. Ongonite from Ongon Khairkhan, Mongolia. Mineralogy and Petrology 43, 255-273.
Syritso, L.F., Badanina, E.V., Abushkevich, V.S., Volkova, E.V., Shuklina, E.V., 2012. Volcanoplutonic association of felsic rocks in the rare-metal ore units of Transbaikalia: Geochemistry of rocks and melts, age, and P-T conditions of their crystallization. Petrology 20, 567-592.
Taylor, R.P., 1992. Petrological and geochemical characteristics of the Pleasant Ridge zinnwaldite-topaz granite, southern New Brunswick, and comparisons with other topaz-bearing felsic rocks. The Canadian Mineralogist 30, 895-921.
Thomas R., 1982. Ergebnisse der thermobarogeochemischen Untersuchungen an Flüssigkeitseinschlüssen in Mineralen der postmagmatischen Zinn-Wolfram-Mineralisation des Erzgebirges. Freiberger Forschungshefte C370, 85 p.
Thomas, R., Davidson, P., Rhede, D., Leh, M., 2009. The miarolitic pegmatites from the Konigshain: a contribution to understanding the genesis of pegmatites. Contributions to Mineralogy and Petrology 157, 505-523.
Thomas, R., Förster, H.-J., Rickers, K., Webster, J.D., 2005. Formation of extremely F-rich hydrous melt fractions and hydrothermal fluids during differentiation of highly evolved tin-granite magmas: a melt/fluid-inclusion study. Contribution to Mineralogy and Petrology 148, 582-601
Walrafen, G.E., 1964. Raman spectral studies of water structure. Journal of Chemical Physics 40, 3249-3256.

Wasim, M., Wasim, M., Zafar, W., Tufail, M., Arif, M., Daud, M., Ahmad, A. 2011. Elemental analysis of topaz from northern areas of Pakistan and assessment of induced radioactivity level after neutron irradiation for color induction. Journal of Radioanalytical & Nuclear Chemistry 287, 821-826.

Watt, G.R., Wright, P., Galloway, S., McLean, C., 1997. Cathodoluminescence and trace element zoning in quartz phenocrysts and xenocrysts. Geochimica Et Cosmochimica Acta 61, 4337-4348.

Webster, J., Thomas, R., Förster, H.-J., Seltmann, R., Tappen, C., 2004. Geochemical evolution of halogen-enriched granite magmas and mineralizing fluids of the Zinnwald tin-tungsten mining district, Erzgebirge, Germany. Mineralium Deposita 39, 452-472

Zhang, R.Y., Liou, J.G., Shu, J.F., 2002. Hydroxyl-rich topaz in high-pressure and ultrahigh-pressure kyanite quartzites, with retrograde woodhouseite, from the Sulu terrane, eastern China. American Mineralogist 87, 445-453.

Figure captions

Fig 1. Photomicrographs (**A** and **C** parallel transmitted light; **B**, **D**, **E** and **F** back-scattered electron image of sample AB1). **A** Phenocrysts of topaz (Toz), K-feldspar (Kfs) and mica in a quartz-feldspar-topaz groundmass. Pl (Na-)plagioclase, cb carbonate. **B** Topaz-hosted inclusion of a Na-Al-F phase, possibly originally included as melt, identified by Raman spectroscopy as cryolithionite [$Na_3Li_3Al_2F_{12}$] (main peak at ~567 cm^{-1}) (crl). A fine-grained Ca-K-bearing crystalline phase is also present. **C** Zoned mica phenocryst showing BSE brightness variations. The BSE-darker rim contains less Fe and more F than the BSE-brighter core. Fl fluorite. **D** Aggregate of radially-arranged W-ixiolite needles included in topaz. **E** Fine-grained groundmass containing quartz, feldspar, topaz, mica and minor monazite (Mnz). **F** Pocket of Ca-carbonate (cb) containing inclusions of fluorite (Fl) and an Al-Si mineral, possibly kaolinite (kaol)

Fig 2. Cathodoluminescence (CL) textures of topaz and quartz phenocrysts. **A** Mosaic of three CL images of a topaz phenocryst. Variations of CL intensities indicate euhedral growth textures and truncations of these (arrowed), indicating growth and resorption events. **B** and **C** (and inset) CL and parallel transmitted light images of topaz phenocrysts. Topaz phenocrysts have rims containing abundant quartz inclusions. **D** and **E** CL images of quartz phenocrysts indicate euhedral growth textures. Note prominent sector zoning. Round healed cracks (arrowed) appear as either dark or bright CL bands

Fig 3. **A** (and insets) Multiple topaz-hosted melt inclusions occurring along trapping plane. The melt inclusions contain silicate glass (gl) and a bubble (V). In addition, several inclusions also contain a colourless anhedral phase identified as cryolithionite [$Na_3Li_3Al_2F_{12}$] by Raman spectroscopy. **B** Topaz-hosted isolated melt inclusions co-trapped with needle-like crystals of W-ixiolite. The inclusions contain glass, vapour (one or multiple bubbles), a cubic crystal (cryolithionite), and unidentified fine-grained colourless crystals. **C** Large, isolated (primary) subhedral quartz-hosted melt inclusion containing silicate glass, a large bubble, an unidentified yellow mineral with cleavage system (inset) and a fine-grained dendritic crystal. **D** Anhedral quartz-hosted melt inclusion containing glass, bubble and an unidentified opaque mineral. Note small fluid inclusions (arrowed). **E** Quartz-hosted multiphase inclusion containing round Y-bearing fluorite (see X-ray elemental maps), silicate glass and a bubble

Fig 4. Plots of major element analyses of melt inclusion glass. Symbol abbreviations: Quartz – subhedral quartz-hosted melt inclusions, Topaz – topaz-hosted melt inclusions, Quartz-II – irregular quartz-hosted melt inclusions, liter – previous analyses (Antipin et al., 2009; Peretyazhko and Savina, 2010a). Arrows indicate the compositional effect of cryolithionite separation, numbers indicate fraction of melt crystallised. Previous analyses have been carried out on homogenised melt inclusions, which may have resulted in SiO_2 addition from the host quartz. Analyses of melt inclusions homogenised at high-temperature (950°C) are not plotted here

Fig 5. Photomicrographs and PIXE maps of **A** topaz-hosted melt inclusions; **B** euhedral quartz-hosted melt inclusion (image in boxed area is located at a different focal depth); **C** irregular-shaped quartz-hosted melt inclusion. Fine daughter crystals in A contain K, Fe, Mn, Cu and Zn. Fine-grained crystals on bubble in C contain Fe-Mn-Cu-Zn-bearing minerals possibly precipitated from vapour in the bubble. Note Mo-K-Fe distribution along crack in C (bottom left)

Fig 6. Fluorine compositions (**A**) and P vs. Si plot (**B**) of topaz phenocrysts (electron microprobe analyses, plotted as wt.%, results from 12 traverses). Cores and rims are distinguished

Fig 7. **A** and **B** CL images and time-resolved LA-ICP-MS traverses of topaz phenocrysts. Dashed lines mark the core-rim contact and the grain margin. Arrows indicate position and direction of LA-ICP-MS traverse

Fig 8. Trace element compositions of topaz phenocrysts (results from 6 traverses). Cores and rims are distinguished. Lithium and B are compared with compositions of topaz from different environments (data from Hervig et al., 1987), Ga values (Max, min, avg) are compared with topaz from granite of the Krušné Hory/Erzgebirge area (Breiter et al., 2013)

Fig 9. Conceptual model for the formation of magmatic topaz and deposition of Nb-Ta-W-oxides in the Ary-Bulak massif

Supplementary Fig 1. Photomicrographs and Raman spectra of glass and minerals. Black crosses indicate position of Raman spectra. **A** (and inset) Raman spectrum of topaz phenocryst showing peak at 3653 cm^{-1} (OH stretching vibration). **B** Topaz-hosted melt inclusions containing silicate glass, vapour bubble and cryolithionite, and Raman spectrum indicating peaks at 356, 398 and 567 cm^{-1} (cryolithionite). **C** Topaz-hosted melt inclusion (silicate glass, vapour bubble and cryolithionite). The high-frequency portion of a Raman spectrum of glass shows a broad peak at 3200 – 3500 cm^{-1} (H_2O vibrational mode). **D** Magmatic fluorite co-trapped with silicate glass in quartz phenocryst

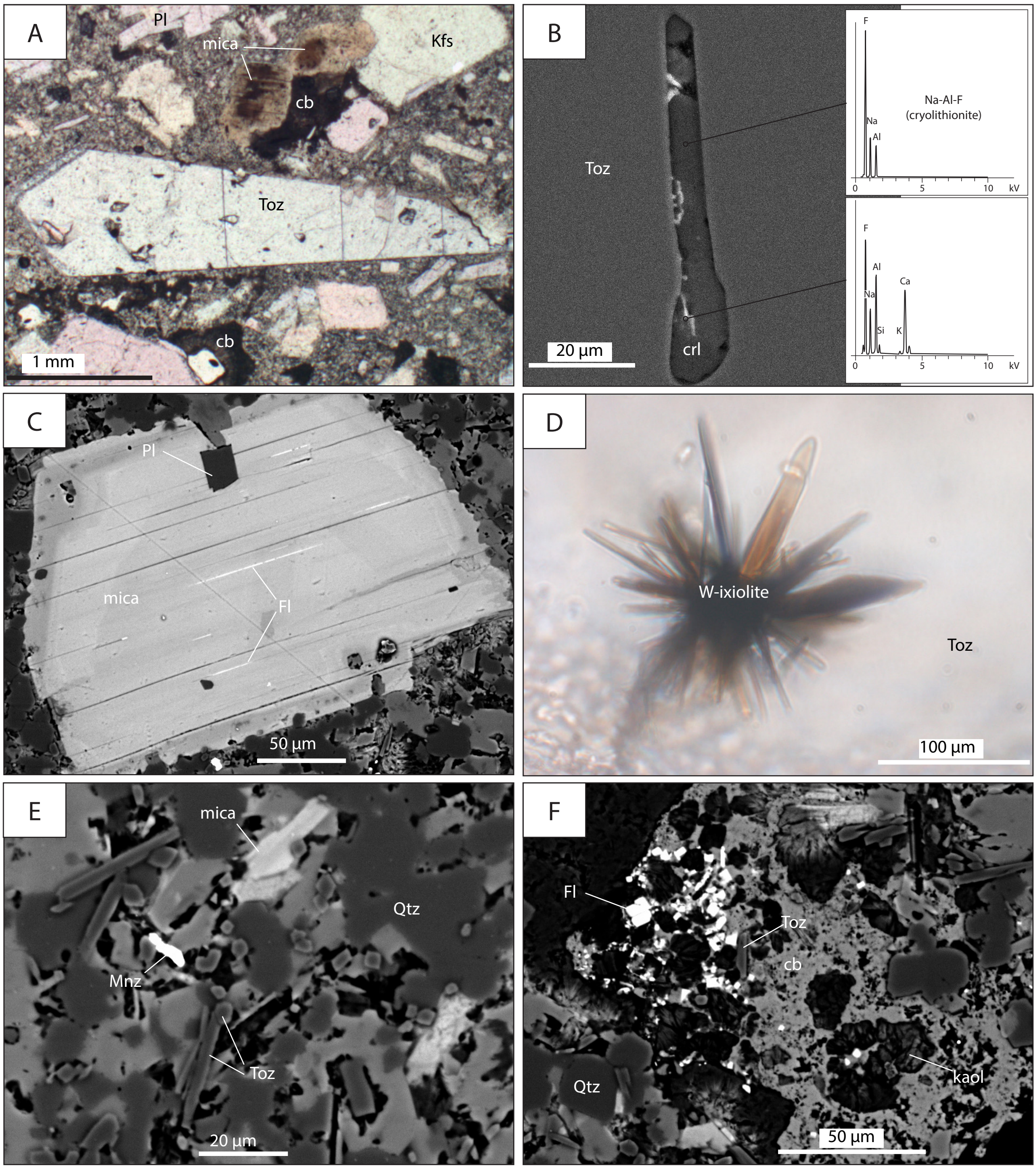

A
Pl
mica
Kfs
cb
Toz
cb
1 mm
B
Toz
Na-Al-F
(cryolithionite)
F
Na
Al
Ca
Si
K
0
5
10
kV
crl
20 µm
C
Pl
mica
Fl
50 µm
D
W-ixiolite
Toz
100 µm
E
mica
Qtz
Mnz
Toz
20 µm
F
Fl
Toz
cb
kaol
Qtz
50 µm

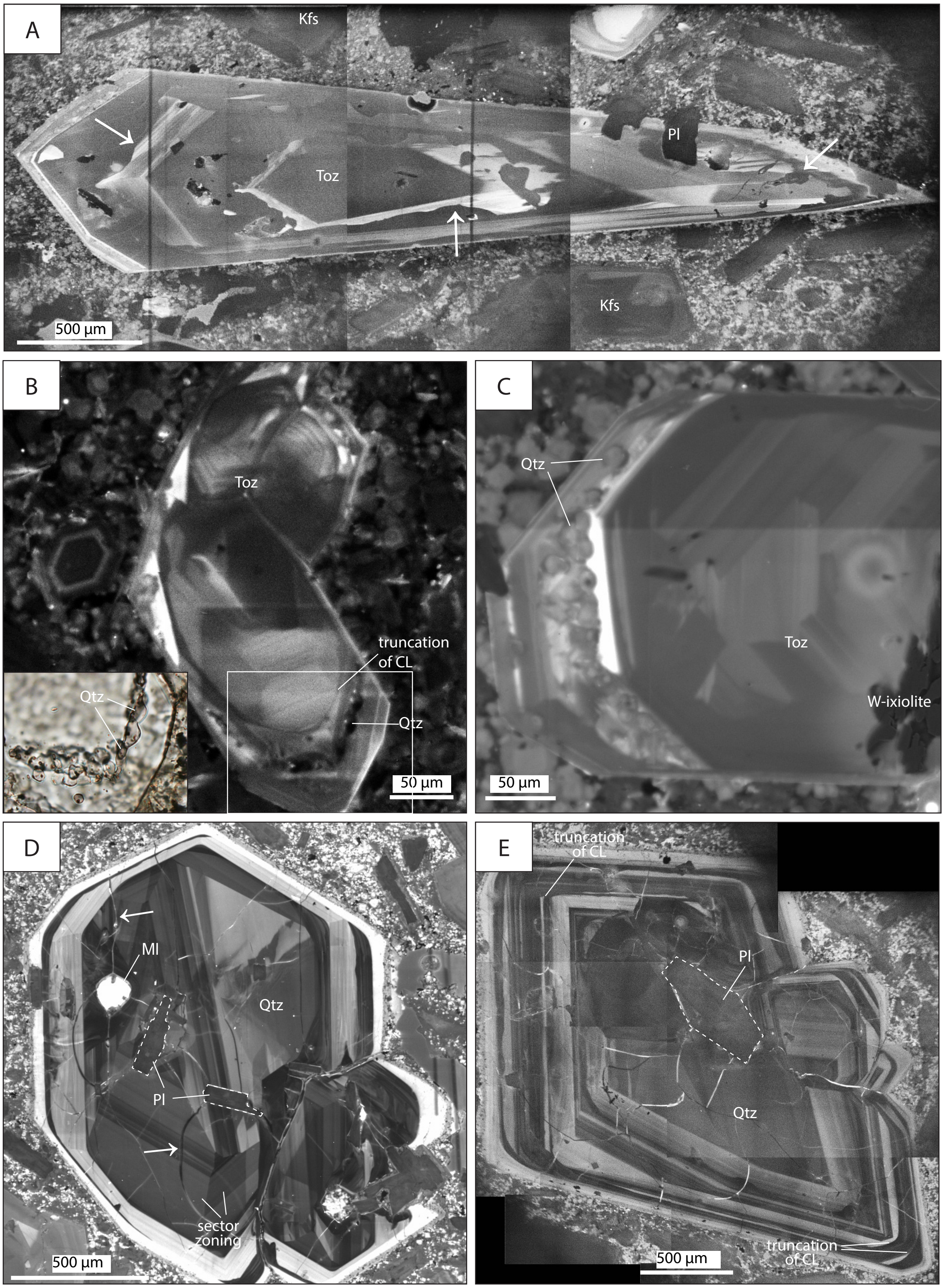

A
Kfs
Toz
Pl
Kfs
500 µm
B
Toz
truncation of CL
Qtz
Qtz
50 µm
C
Qtz
Toz
W-ixiolite
50 µm
D
MI
Qtz
Pl
sector zoning
500 µm
E
truncation of CL
Pl
Qtz
truncation of CL
500 µm

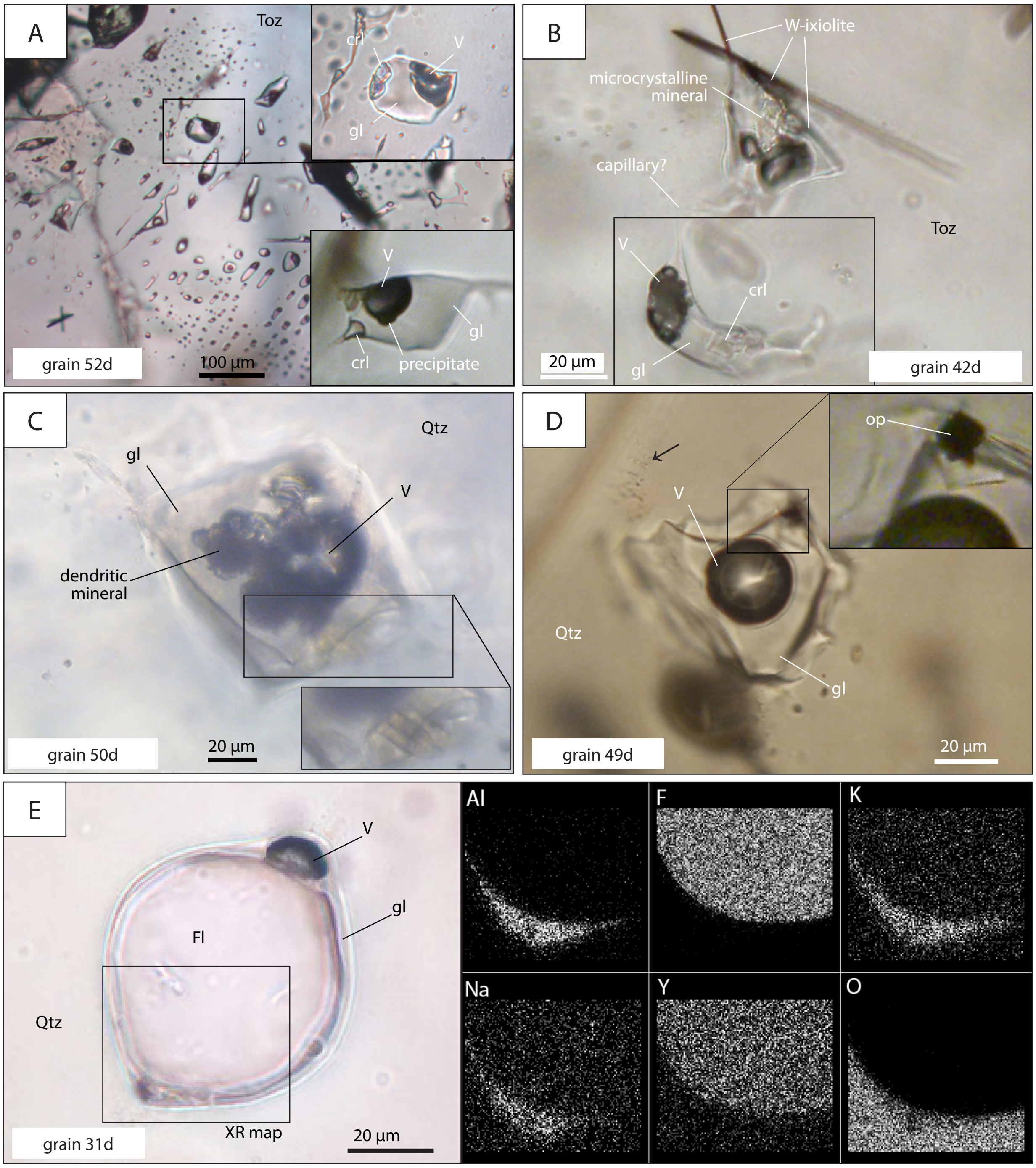
A
Toz
crl
V
gl
V
gl
crl
precipitate
grain 52d
100 µm
B
W-ixiolite
microcrystalline mineral
capillary?
Toz
V
crl
gl
20 µm
grain 42d
C
Qtz
gl
V
dendritic mineral
grain 50d
20 µm
D
op
V
Qtz
gl
grain 49d
20 µm
E
V
gl
Fl
Qtz
grain 31d
XR map
20 µm
Al
F
K
Na
Y
O

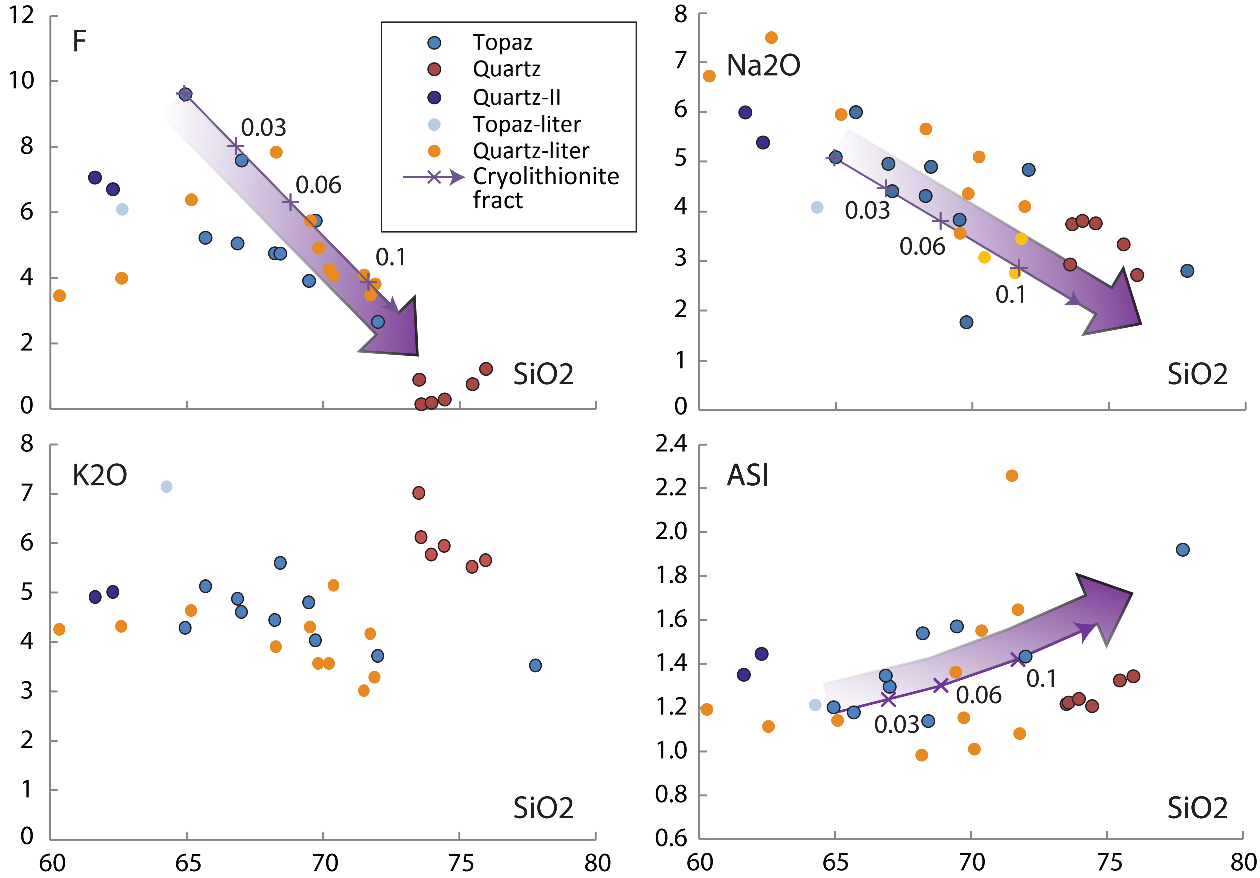

F
Na2O
K2O
ASI
SiO2
SiO2
SiO2
SiO2
Topaz
Quartz
Quartz-II
Topaz-liter
Quartz-liter
Cryolithionite fract
0.03
0.06
0.1
0.03
0.06
0.1
0.03
0.06
0.1

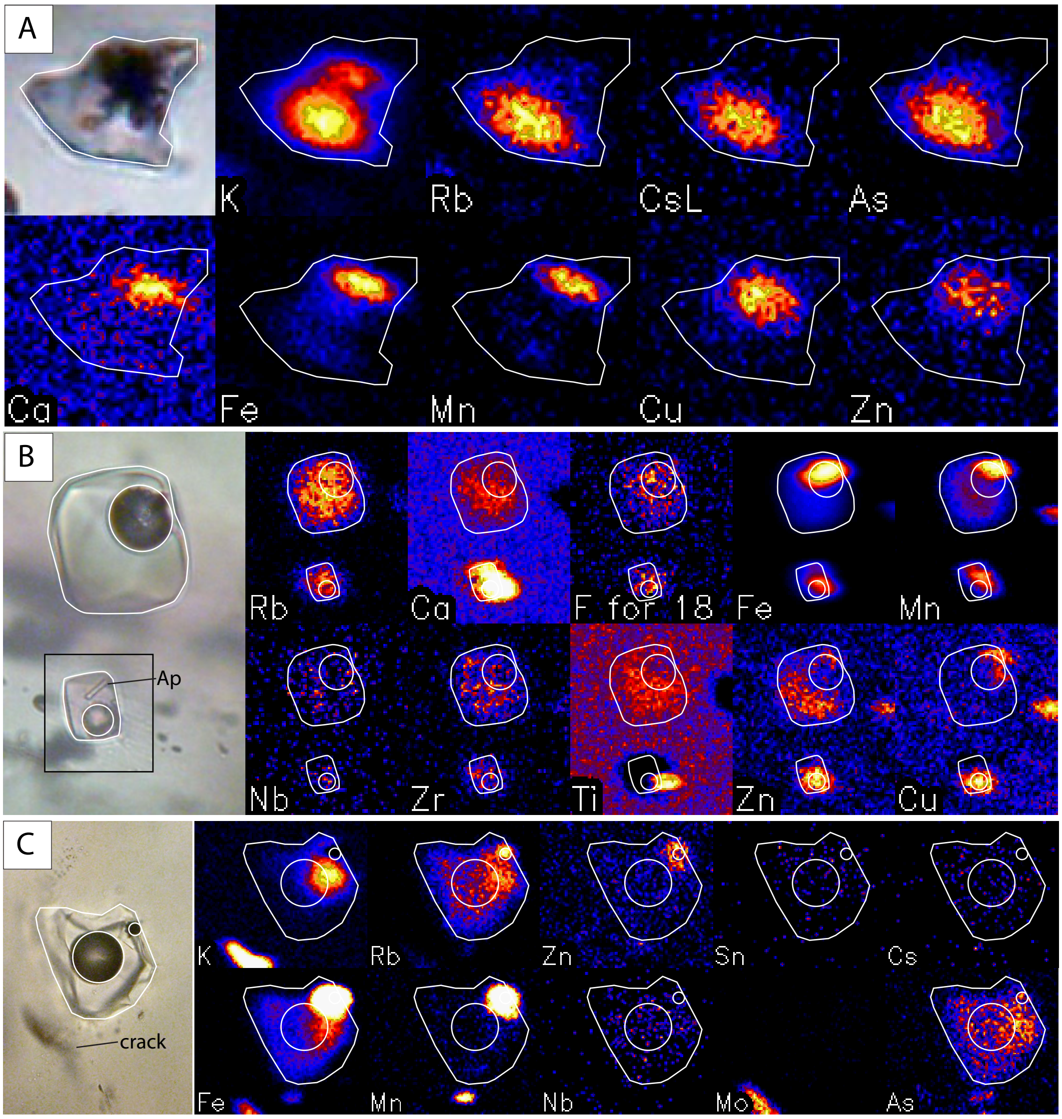
A
K
Rb
CsL
As
Ca
Fe
Mn
Cu
Zn
B
Ap
Rb
Ca
F for 18
Fe
Mn
Nb
Zr
Ti
Zn
Cu
C
crack
K
Rb
Zn
Sn
Cs
Fe
Mn
Nb
Mo
As

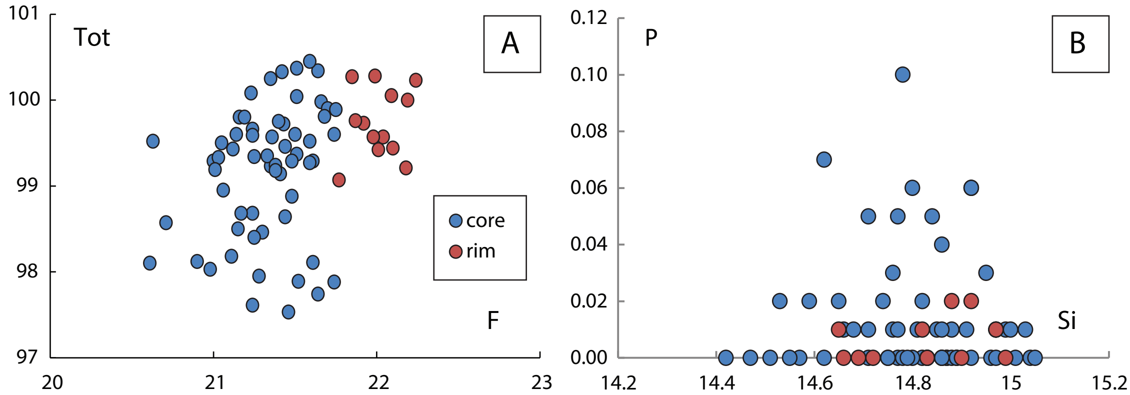

101
100
99
98
97
Tot
A
core
rim
F
20
21
22
23
0.12
0.10
0.08
0.06
0.04
0.02
0.00
P
B
Si
14.2
14.4
14.6
14.8
15
15.2

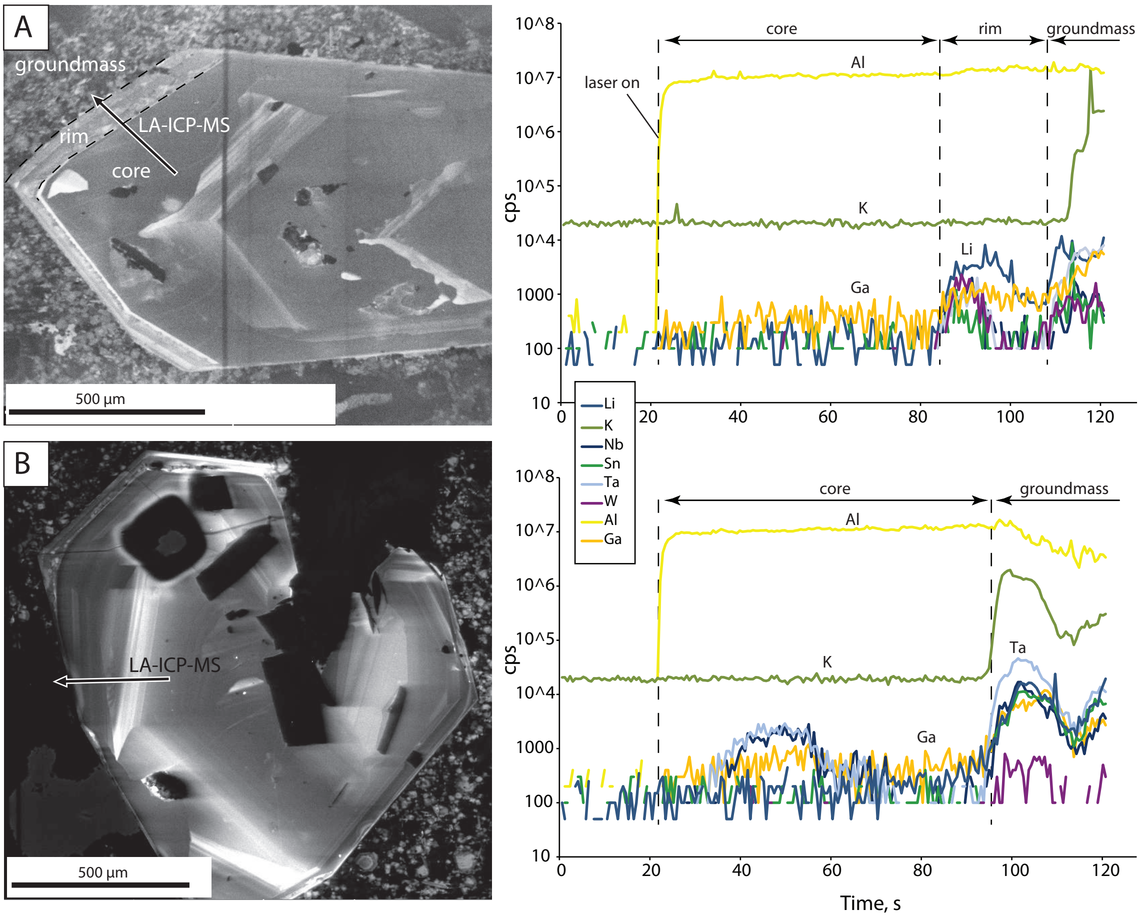

A
groundmass
rim
LA-ICP-MS
core
500 µm
B
LA-ICP-MS
500 µm
core
rim
groundmass
laser on
Al
K
Li
Ga
Ta
cps
Time, s
Li
K
Nb
Sn
Ta
W
Al
Ga

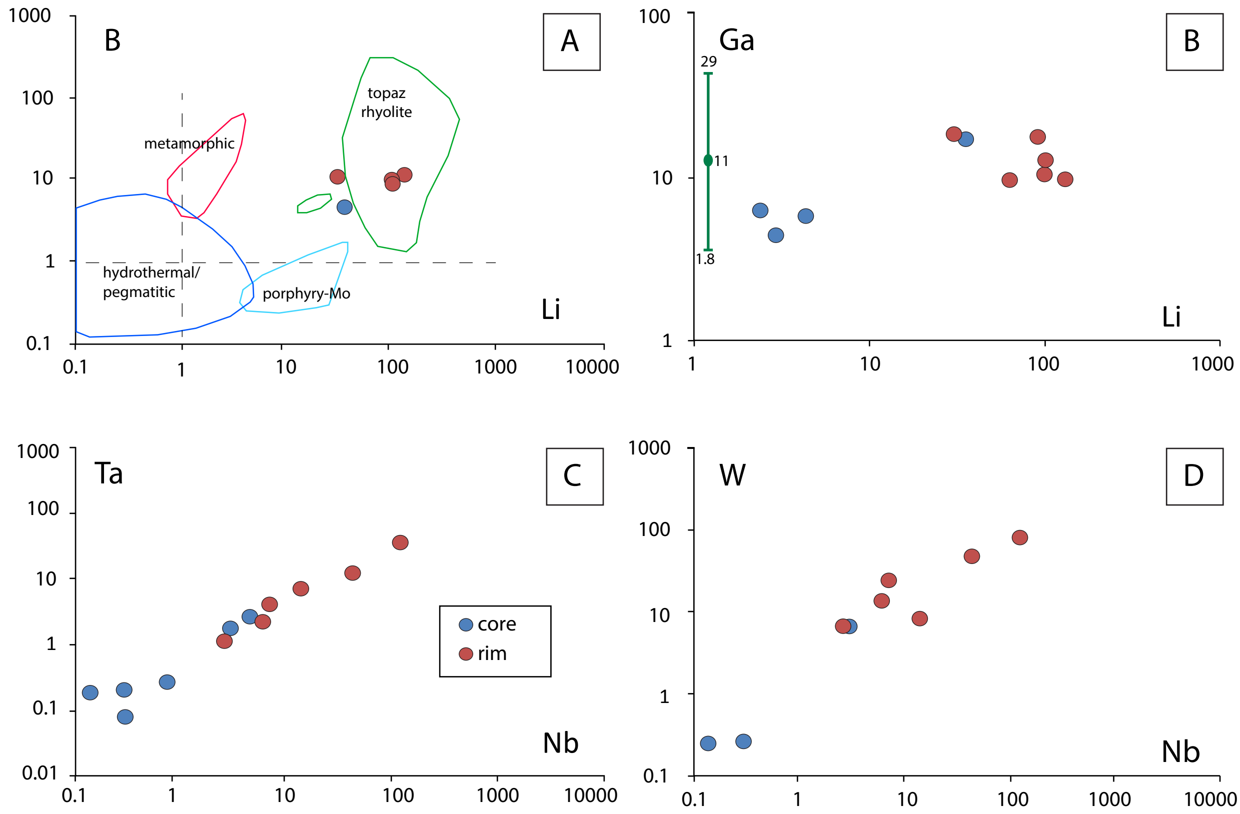
A
B
Li
metamorphic
topaz
rhyolite
hydrothermal/
pegmatitic
porphyry-Mo
1000
100
10
1
0.1
0.1
1
10
100
1000
10000
B
Ga
Li
29
11
1.8
100
10
1
1
10
100
1000
C
Ta
Nb
core
rim
1000
100
10
1
0.1
0.01
0.1
1
10
100
1000
10000
D
W
Nb
1000
100
10
1
0.1
0.1
1
10
100
1000
10000

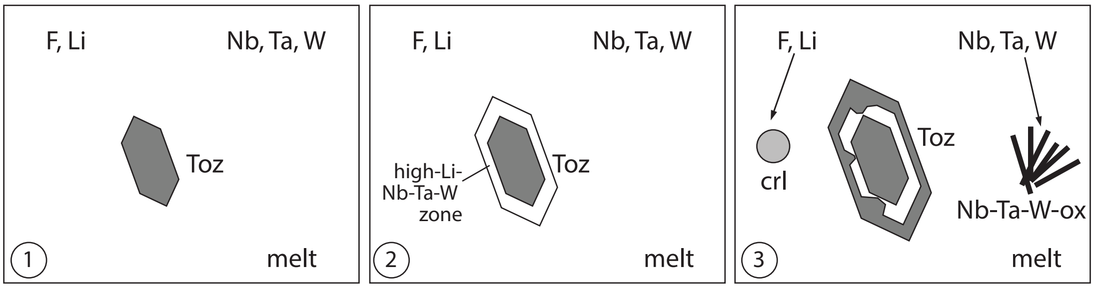

1. Nb, Ta and W are progressively concentrated in the melt during fractionation of high-F-Li magma

2. Growth stages of topaz with different trace element contents record the compositional evolution of the melt

3. Separation of cryolithionite depletes the melt in F and Li, thus depressing the solubility of Nb, Ta and W, and causing their deposition as oxides. Strong F depletion may destabilise topaz and cause resorption